THE JOURNAL OF PHYSICAL CHEMISTRY C

Article

Cite This: J. Phys. Chem. C 2018, 122, 422−428

pubs.acs.org/JPCC

Soft Templating of Water Aggregates Disrupts $\pi-\pi$ Stacking in Crystalline Poly(3-hexylthiophene)

Kshitij C. Jha, Alexander Weber, Yeneneh Y. Yimer,† and Mesfin Tsige*

Department of Polymer Science, The University of Akron, Akron, OH 44325, United States

Supporting Information

ABSTRACT: The $\pi-\pi$ stacking robustness of the photoactive layer is key to maintaining efficiency of organic photovoltaics (OPVs). We show local disruption more than 2 Å on average in the $\pi-\pi$ stack of crystalline poly(3-hexylthiophene) (P3HT), one of the most common materials used in OPVs, through formation of a chainlike water structure with limited growth and mostly pentameric cluster ends. In contrast, a 3D aggregated water cluster with constant growth is observed in amorphous P3HT. Dynamics of water molecules that form the largest aggregates in crystalline P3HT show the effect of limited mobility, when compared to amorphous P3HT, due to dual confinement from both alkyl side groups and thiophene backbone. We term this dual confinement *soft templating* and quantify its effect on nature, size, and hydrogen bond participation of water aggregates in crystalline and amorphous P3HT using all-atom molecular dynamics with in-house developed potentials that were previously shown to represent the interfacial and wetting behavior of P3HT systems in good agreement with experiments. Examination of disruption behavior presented for P3HT would allow smart molecular design of photoactive layers.

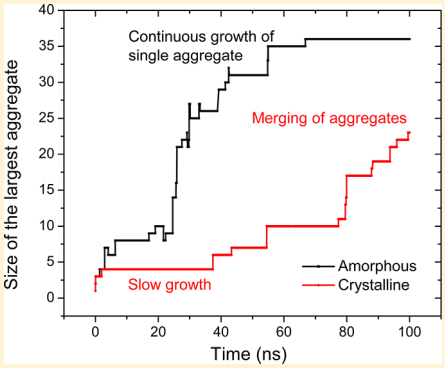

INTRODUCTION

Boosting the lifecycle of organic photovoltaics (OPVs) is key to increasing their market adoption. A major barrier to increments in OPV lifecycle is diffusion of water and solvents, which have been demonstrated as being a significant cause of degradation. Water and solvent atmosphere guided diffusion inside OPVs and their subsequent degradation has been extensively studied.[1−4] Mechanisms that contribute to loss in OPV efficiency include disruption of electron donor pathways, and reactive degradation and delamination at functional interfaces. While all of these mechanisms that lead to loss in efficiency would depend on water and solvent clustering effects, deviations from $\pi-\pi$ stacked geometries of the photoactive layer especially impede electron transfer, and is the focus of this article for the case of poly(3-hexylthiophene) (P3HT). To our knowledge, this is the first report of the water aggregate formation pathway in P3HT matrices at a molecular level.

Our current understanding of water microaggregate formation is based on wide-ranging investigations that have quantified hydrogen bond and coordination dynamics under confinement in carbon nanotubes,[5,6] graphite,[7,8] metal−organic frameworks,[9] hydrogels,[10,11] silica,[12] zeolite,[13] supramolecular structures,[14,15] and polymeric melt.[16] Variations in the nature of confinement, such as soft (polymer and self-assembled monolayers) vs hard (zeolites and silica), and patterned (graphite and carbon nanotubes) vs random (hydrogels), lead to large changes in structure and dynamics of confined water. Changes in the organization and evolution of water aggregates and bound water have practical implications for membrane transport,[17−19] protein folding,[20−22] adhesion of biomacromolecules,[23−25] design of anti-icing surfaces,[26−28] selective organic remediation,[29−32] and oil recovery.[33−35]

In view of the recent interest in dynamics of water under soft confinement,[36] the P3HT framework presents a unique molecular structure where confinement occurs from both the alkyl side groups and thiophene backbone. The confinement from the alkyl groups is soft and fluctuating due to the nature of the motion of the aliphatic chains. The confinement from the thiophene backbone is structured and more rigid. The dual nature of confinement from the framework leads to interesting water aggregation effects exhibited in dynamics, coordination, and hydrogen bond participation that can be contrasted to the amorphous P3HT matrix.

METHODS

All-atom molecular dynamics (MD) simulations are used to quantify the behavior of water confinement in crystalline and amorphous P3HT. The potentials for all-atom MD were developed in-house and have been validated through comparison to interfacial and bulk structure of P3HT[37−39] as well as its wettability.[40]

For crystalline P3HT, there are 64 chains containing 20 monomers from each simulation box with $\pi-\pi$ stacking along the *y*-axis. The short-chain P3HT provides an overview on the dynamics of water inside a soft templated organic material. It is worth mentioning that even slight changes in tacticity for

Received: September 14, 2017
Revised: December 7, 2017
Published: December 8, 2017

DOI: 10.1021/acs.jpcc.7b09191
J. Phys. Chem. C 2018, 122, 422−428

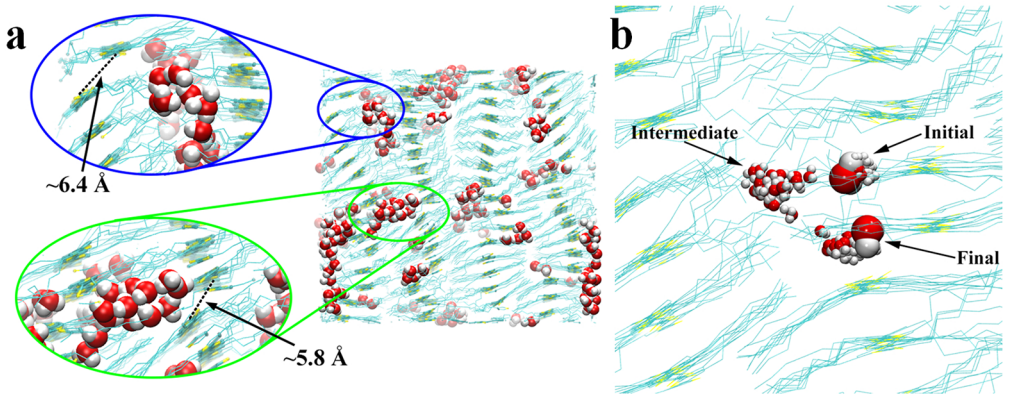

Figure 1. Panel (a) is a representative image of the disruption in $\pi-\pi$ stacking caused by water aggregation in the crystalline P3HT matrix. The broken lines show the new stack distances, which are significantly larger than the equilibrium value of 3.8 Å, with two illustrative values of 5.8 and 6.4 Å. Panel (b) depicts the characteristic "hopping" of a water molecule in a crystalline P3HT system between three states. Each water molecule is a point in the trajectory over a simulation time of approximately 1.4 ns. Water molecules were chosen to best highlight the trajectory. The molecules representing the initial and final points in the trajectory are shown with larger van der Waals radii.

common polymers,[41−50] as well as P3HT,[51−54] may lead to large differentials in physical behavior. Along these lines, maintenance of regioregularity and processability is a concern for P3HT at higher molecular weights[55,56] and analyzing a 20-mer would allow for quantification of the disruption in $\pi-\pi$ stacking to be accessed while keeping other factors constant. Furthermore, the packing of the crystalline P3HT is stable and can be represented even by a 10 monomer form and the densities change only by 2% going from a 10-mer to infinite chain length.[39] Torsional population for planar backbone and hexyl side chains converges at a 20-mer chain length.[39] A 20-mer chain, with a stable and representative packing, allows for two chains in the lateral direction and is a reasonable system size to explore the underlying local mechanism that depends only on the nature of the soft templating induced by the crystal structure.

The potentials used correctly replicated the 3.8 Å[39] distance between $\pi-\pi$ stacks, observed from diffraction studies.[57] The ordering of the backbone and hexyl chains was along the *x*- and *z*-axes, respectively. The distance between the alkyl side groups (4 Å) is of the same order as the distance between the thiophene backbone (3.8 Å). Hence, crystalline P3HT exhibits dual confinement in the *x*- and *y*-directions. For amorphous P3HT, the number of chains and monomers remained the same as the crystalline case. A 12-6 van der Waals potential with a cutoff of 12 Å was applied for all systems. The developed potentials were based on optimized potentials for the liquid simulations-all-atom (OPLS-AA) paradigm. Details of force field parameters and potential energy functions are provided in section S1 of the Supporting Information. Long range Coulomb interactions were computed using the particle-particle/particle-mesh (PPPM) Ewald algorithm.[58] All simulations were carried out at 300 K using the Large-scale Atomic/Molecular Massively Parallel Simulator (LAMMPS) package developed and maintained by Sandia National Laboratories.[59]

To test the saturation limit of the P3HT systems, water molecules varying in number from 20 to 200 were dispersed within the two P3HT matrices. The dispersion of water molecules inside the P3HT matrix was done randomly, while avoiding overlap with any other atoms so that no artificial imperfections are created in the system. Differentials in the nature of water confinement and aggregation between the crystalline and amorphous systems was best represented by the choice of 200 water molecules in the simulation box, which distinctly portrayed stability in the largest water aggregate formed for crystalline P3HT, and continuous growth for amorphous P3HT (see Abstract image). The number of water molecules is seen as sufficient to study the mechanism of $\pi-\pi$ disruption and the effect of aggregate formation due to dual templates. More water molecules would cause more disruption. All trajectories represent a simulation time of 100 ns.

RESULTS AND DISCUSSION

A major characteristic of the water aggregate in crystalline P3HT, as shown in Figure 1a, is its chainlike nature with end termination by larger sized "head groups". We term these terminal "head groups" as *end clusters*. These *end clusters* are primarily responsible for the disruption in $\pi-\pi$ stacking. Also noticeable is the local disruption caused around a $\pi-\pi$ stack that has been displaced from its equilibrium value of 3.8 Å. This points to a dynamic nature of the chainlike water aggregates in crystalline P3HT, with *end clusters* that disrupt a number of adjacent sites. An increase in $\pi-\pi$ stacking distance of up to 2.6 Å from equilibrium value has been observed. The effect of such $\pi-\pi$ disruptions is directly related to loss in electron transfer pathways and efficiency, previously shown through DFT computations to occur for displacements in $\pi-\pi$ stack distance for values as small as 0.5 Å.[60] Additionally, displacement of the $\pi-\pi$ stack would also be typically accompanied by angular distortion, which would further decrease the efficiencies. At the same time, in the absence of other water clusters around the $\pi-\pi$ stack, we would expect reversion to the minimum energy $\pi-\pi$ stacked state.

What leads to this unique water aggregate geometry for the crystalline P3HT? We hypothesize that the total size of the water aggregate is limited for crystalline P3HT because of the dual confinement inherent to the molecular framework. The alkyl side groups push the water molecules toward their limiting size, through a soft fluctuating confinement. The distance between the alkyl side groups (4 Å) is of the same order as the distance between the thiophene backbone (3.8 Å). Hence, twin confinement leads to the unique chainlike structure with *end cluster* termination.

Further, for individual water molecules, loss in mobility in a crystalline matrix would mean a lower probability of joining a water aggregate as part of the chain or *end cluster*. In glassy and

DOI: 10.1021/acs.jpcc.7b09191
J. Phys. Chem. C 2018, 122, 422−428

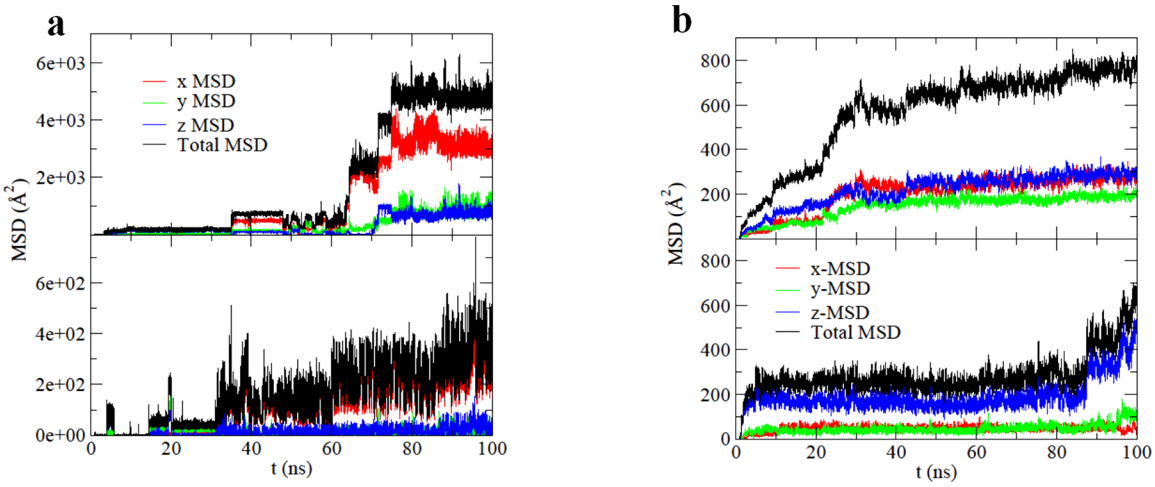

Figure 2. Panel (a) shows MSD values for a representative water molecule that never joined a water aggregate during 100 ns of the simulation for amorphous (top) and crystalline (bottom) P3HT matrices. The representative water molecule for crystalline P3HT is the same water molecule for which "hopping" is illustrated in Figure 1b. The representative water molecule for amorphous P3HT is 1 of only 3 water molecules, out of 200, that never joined a water aggregate. Panel (b) shows MSD values for water molecules constituting the largest water aggregate for amorphous (top) and crystalline (bottom) P3HT matrices.

crystalline polymers, water diffusion is known to exhibit a "hopping" mechanism, wherein an examination of spatial trajectories shows confinement within "cavities", with an occasional jump from one cavity to another that is very fast—of the order of picoseconds.[61] The "hopping" motion is a direct consequence of the packing of polymers. The three states of a "hopping" water molecule, with the molecule being selected such that it is free throughout the 100 ns trajectory and never joined a water aggregate, is shown in Figure 1b. The trajectory represents motion between 13 and 14.4 ns for the representative water molecule. The jump to the intermediate "cavity" is quick (within 4−6 ps), where it stays for less than 50 ps, followed by movement to the final state where it stays for several nanoseconds before making another jump.

How would the behavior for a free water molecule differ between amorphous and crystalline P3HT matrices? What does the dynamics of the free water molecule tell us about the nature of the water aggregates/clusters in both matrices?

To answer the above, mean-squared displacement (MSD) calculations were carried out for (i) a single representative water molecule that never joined any aggregate or cluster throughout the 100 ns trajectory in amorphous and crystalline P3HT, and (ii) all water molecules that form the largest water aggregate in amorphous and crystalline P3HT matrices tracked from the initial time $t = 0$.

Figure 2a shows the single free water molecule MSD for amorphous (top) and crystalline (bottom) matrices. The "hopping" between "cavities" is more frequent for the amorphous P3HT matrix, and the absolute values for MSD are an order of magnitude greater than that for crystalline P3HT. The limited mobility of the free water molecule in crystalline P3HT, in comparison to amorphous P3HT, reduces their probability of joining a water aggregate as discussed above. This would point to a larger water aggregate for the amorphous P3HT matrix. Also shown in the MSD values in Figure 2a is the signature of the "hopping" between states. The MSD for a single free water molecule in crystalline P3HT represents the same molecule for which "hopping" was shown in Figure 1b. The "hop" from intermediate to final state is in the range of the second jump in MSD values and illustrates the quick nature of the process.

Figure 2b shows the MSD for all water molecules that constitute the largest aggregate for amorphous (top) and crystalline (bottom) P3HT matrices. It is apparent that the confinement effects are not anisotropic (or directional) for the set of water molecules constituting the amorphous P3HT matrix. The dual confinement due to the thiophene backbone and alkyl side chains is illustrated in hindered dynamics for the set of water molecules forming the largest aggregate for the crystalline P3HT matrix. For the crystalline case, we observe an order of magnitude higher diffusion in the z-direction, pointing to marked anisotropy due to dual confinement. There is a distinct contrast of the anisotropic diffusion behavior of water molecules constituting the largest aggregate in the crystalline P3HT matrix with the nearly similar diffusion in all three directions for water molecules constituting the largest aggregate in the amorphous P3HT matrix.

A further examination of the MSD behavior of the largest aggregate in the crystalline P3HT matrix (Figure 2b, bottom) reveals an initial fast dynamics, before 10 ns, where the largest aggregate is formed. Formation of the initial aggregate before 10 ns can also be observed in the Abstract image. Initial formation is followed by a slow dynamics region up to 80 ns where the aggregate moves as a whole. In this middle portion of the MSD (Figure 2b, bottom), the largest aggregate is moving toward the crystal edge (chain ends) with slow dynamics, and causes local disruptions in the $\pi-\pi$ stacking with its movement. Local disruption effects can be seen in Figure 1a. Beyond 80 ns, as the movement of the aggregate proceeds to the region between the 20-mer chain ends, more free volume is available. The availability of larger free volume at the chain ends leads to faster dynamics and merging of aggregates as can be seen in the increase in size of aggregate for the crystalline matrix after 80 ns (Abstract image). Increase in molecular weight of P3HT would increase the time at which the aggregate starts to move as a whole and meet the chain ends. The nature of the aggregate, however, would remain the same. In this context, we have also analyzed the wettability of 20-mers and 40-mers and found that the effect of chain length is minimal in terms of changes in

DOI: 10.1021/acs.jpcc.7b09191
J. Phys. Chem. C 2018, 122, 422−428

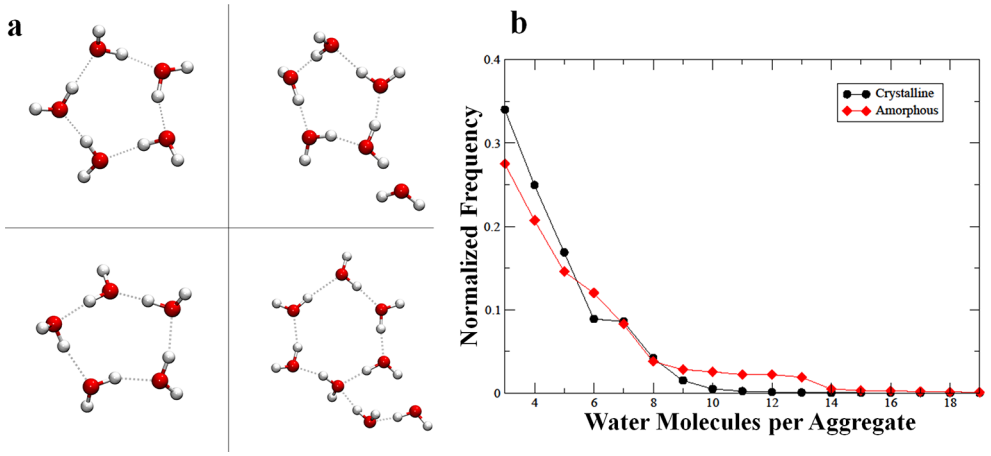

Figure 3. Panel (a) shows the nature of *end clusters* that terminate the chainlike water aggregate for crystalline P3HT. The majority of the *end clusters* in crystalline P3HT are pentameric, although there are other forms such as hexamer (shown) and tetramer (not shown). Panel (b) shows the aggregate size distribution presented as normalized frequencies for crystalline and amorphous P3HT averaged for the last 1 ns of the simulation.

interfacial energies[40] with the exposure of backbone versus side chain being the dominant influence in wettability. Hence, a stable packed 20-mer would mechanistically represent the diffusion inside as well as the local aggregation leading to $\pi-\pi$ disruption in crystalline P3HT. Additionally, the behavior after 80 ns does not directly contribute to the disruption in $\pi-\pi$ stacking, since the aggregate, though much larger due to merging with other aggregates, is out of the soft confinement region.

The *end clusters* in these slow moving aggregates in crystalline P3HT are the cause of $\pi-\pi$ stacking disruption. The nature of the *end clusters* is important in understanding the extent of disruption. Figure 3a shows various forms of the *end clusters*, with a higher number of cyclic pentamer forms. The *end clusters* switch back and forth between pentameric, hexameric, and tetrameric forms (see the Supporting Information for the movie) which point toward these three being thermodynamically accessible states. The three clusters (tetra-, hexa-, and penta-) have previously been reported to favor boat, chair, and semichair structures.[62−65] We observe all of these forms in the dynamics of molecules forming *end clusters*. What is unique is the high statistical population of pentameric structures without stabilization from a ligand or an ion.

The structural symmetric forms of the *end clusters* are common in clathrate hydrate formations which have a templated growth mechanism based on initial "caged" molecules.[66,67] The pentameric form has previously been reported as resulting from "hydrophobic ice" like structures[68,69] under confinement, which are different from three-dimensional hexagonal ice-like structures where no confinement exists.[70] The metastable nature of the penatmeric form has also been reported for protein cavities, organic crystals, and supramolecular complexes.[71−73] The pentameric form is hypothesized as the favored configuration. We observe that the presence of water molecules near the pentameric form leads to switches in acceptance and rejections (see the Supporting Information for the movie), and the resultant minimum energy conformations are part of the metastable nature of the *end clusters*. It should be noted that the unique templating in the *x*- and *y*-directions from wagging alkyl chains and rigid thiophene backbone leads to the chainlike metastable pentameric *end cluster* terminated water aggregates in crystalline P3HT matrices.

Figure 3b shows the limits of aggregate size for crystalline P3HT, with a larger number of smaller aggregates. This is consistent with our observation that dual confinement and lowered mobility of free water molecules lead to lowered water aggregate sizes for crystalline P3HT. The aggregates in amorphous P3HT continue to grow and are not limited by confinement due to defined packing of chains. The water agglomeration in the amorphous matrix shows an Ostwald ripening mechanism,[74] wherein the smaller aggregates are merged into larger ones.

The significant difference in the nature of water aggregation in amorphous and crystalline P3HT matrices is expected to translate to their hydrogen bond participation. Since the free water molecules are more mobile, and larger aggregates continue their growth (see the Abstract image) for the amorphous matrix, it would be expected that the overall participation rate is higher for amorphous P3HT when compared to crystalline P3HT. This is in fact true (Supporting Information, Figure S1), where the hydrogen bond participation rate saturates to 98% for amorphous P3HT (only 3 free water molecules out of 200 at the end), compared to 90% for crystalline P3HT. The criteria for computing hydrogen bonds are based on our previous work on wetting of chemically modified surfaces.[75]

Since the hydrogen bond participation rates are higher for water molecules, as expected, inside the amorphous P3HT matrix, a breakdown of the type of hydrogen bond over the course of the simulation is needed to further elucidate the aggregation behavior under confinement.

Figure 4 represents the breakdown of the nature of hydrogen bonds for all water molecules inside amorphous and crystalline P3HT. For amorphous P3HT, the increase in 3 hydrogen bonds per water molecule is significant and represents the continuous growth in the size of the amorphous aggregate, since a large number of the water molecules would reside on the surface of the water aggregate. This behavior is accompanied by continuous lowering of 2 hydrogen bonds per water molecule, showing a growth toward a three-dimensional aggregate. For crystalline P3HT, the approximately 10% of water molecules that are free can be seen with 0 hydrogen bonds per water molecule at 100 ns. The growth in the 3 hydrogen bonds per water molecule is due to the *end clusters* and also the merging of aggregates outside of the soft

DOI: 10.1021/acs.jpcc.7b09191
J. Phys. Chem. C 2018, 122, 422−428

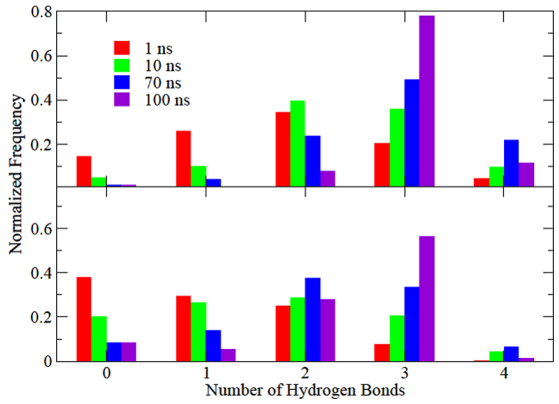

Figure 4. Time evolution of the nature of hydrogen bond for all water molecules, shown in terms of normalized frequencies, inside amorphous (top) and crystalline (bottom) P3HT matrices. Values have been averaged over the last 1 ns of the time period shown in the bargraph.

confinement region. The population of 2 hydrogen bonds per water molecule stabilizes, indicating an equilibrium of the 2-D chainlike structure, with more growth going toward the *cluster ends*.

CONCLUSION

In summary, we report the critical role of the water aggregation under confinement in disrupting the $\pi-\pi$ stacking of crystalline P3HT. Slow dynamics of the *end cluster* in crystalline P3HT allows for large local disruptions. The MSD behavior of the free water molecules shows mobility in the amorphous matrix being an order of magnitude larger than that in the crystalline matrix. The "hopping" behavior in the crystalline matrix is a fast transfer (in the order of ps) between various "cavities", in line with previously reported behavior, followed by extended residence in "cavities" when compared to the amorphous matrix. Dual confinement and impeded mobility limit the aggregate size growth in the crystalline P3HT matrix. The two-dimensional chainlike structure with predominantly pentameric *cluster ends* for crystalline P3HT water aggregates is a result of soft templating from both the thiophene backbone and side chain alkyl side chains. The pentameric end cluster exists in a metastable state and switches to hexameric and tetrameric forms upon acceptance or rejection of proximal water molecules. Design considerations that take into account water aggregation due to changes in confinement resulting from modifications to the backbone and side groups would lead to OPVs with lower degradation.

ASSOCIATED CONTENT

Supporting Information

The Supporting Information is available free of charge on the ACS Publications website at DOI: 10.1021/acs.jpcc.7b09191.

Movie showing the dynamics of *end cluster* for the crystalline P3HT matrix (MPG)

All force field parameters and potential energy functions. Hydrogen bond participation rate for all water molecules inside amorphous and crystalline P3HT matrices over the course of the simulation (PDF)

AUTHOR INFORMATION

Corresponding Author

*E-mail: mtsige@uakron.edu.

ORCID

Kshitij C. Jha: 0000-0002-5354-9852

Mesfin Tsige: 0000-0002-7540-2050

Present Address

†Department of Chemical Engineering, University of Washington, Seattle, WA 98195, United States.

Notes

The authors declare no competing financial interest.

ACKNOWLEDGMENTS

This work was made possible by funding from the ACS Petroleum Research Fund (ACS PRF 54801-ND5) and the National Science Foundation (NSF DMR-1410290).

REFERENCES

(1) Parnell, A. J.; Cadby, A. J.; Dunbar, A. D.; Roberts, G. L.; Plumridge, A.; Dalgliesh, R. M.; Skoda, M. W.; Jones, R. A. Physical Mechanisms Responsible for the Water-induced Degradation of PC61BM P3HT Photovoltaic Thin Films. *J. Polym. Sci., Part B: Polym. Phys.* **2016**, *54*, 141−146.

(2) Norrman, K.; Gevorgyan, S. A.; Krebs, F. C. Water-Induced Degradation of Polymer Solar Cells Studied by H218O Labeling. *ACS Appl. Mater. Interfaces* **2009**, *1*, 102−112.

(3) Wang, W.; Guo, S.; Herzig, E. M.; Sarkar, K.; Schindler, M.; Magerl, D.; Philipp, M.; Perlich, J.; Müller-Buschbaum, P. Investigation of Morphological Degradation of P3HT: PCBM Bulk Heterojunction Films Exposed to Long-term Host Solvent Vapor. *J. Mater. Chem. A* **2016**, *4*, 3743−3753.

(4) Norrman, K.; Madsen, M. V.; Gevorgyan, S. A.; Krebs, F. C. Degradation Patterns in Water and Oxygen of an Inverted Polymer Solar Cell. *J. Am. Chem. Soc.* **2010**, *132*, 16883−16892.

(5) Byl, O.; Liu, J.-C.; Wang, Y.; Yim, W.-L.; Johnson, J. K.; Yates, J. T. Unusual Hydrogen Bonding in Water-Filled Carbon Nanotubes. *J. Am. Chem. Soc.* **2006**, *128*, 12090−12097.

(6) Mashl, R. J.; Joseph, S.; Aluru, N.; Jakobsson, E. Anomalously Immobilized Water: A New Water Phase Induced by Confinement in Nanotubes. *Nano Lett.* **2003**, *3*, 589−592.

(7) Lin, C.; Zhang, R.; Lee, S.; Elstner, M.; Frauenheim, T.; Wan, L. Simulation of Water Cluster Assembly on a Graphite Surface. *J. Phys. Chem. B* **2005**, *109*, 14183−14188.

(8) Cabrera Sanfelix, P.; Holloway, S.; Kolasinski, K.; Darling, G. The Structure of Water on the (0001) Surface of Graphite. *Surf. Sci.* **2003**, *532−535*, 166−172.

(9) Wei, M.; He, C.; Hua, W.; Duan, C.; Li, S.; Meng, Q. A Large Protonated Water Cluster H+ (H2O) 27 in a 3D Metal- Organic framework. *J. Am. Chem. Soc.* **2006**, *128*, 13318−13319.

(10) Faroongsarng, D.; Sukonrat, P. Thermal Behavior of Water in the Selected Starch-and Cellulose-Based Polymeric Hydrogels. *Int. J. Pharm.* **2008**, *352*, 152−158.

(11) Crupi, V.; Majolino, D.; Mele, A.; Rossi, B.; Trotta, F.; Venuti, V. Modelling the Interplay between Covalent and Physical Interactions in Cyclodextrin-Based Hydrogel: Effect of Water Confinement. *Soft Matter* **2013**, *9*, 6457−6464.

(12) He, Y.; Cao, C.; Wan, Y.-X.; Cheng, H.-P. From Cluster to Bulk: Size Dependent Energetics of Silica and Silica-Water Interaction. *J. Chem. Phys.* **2006**, *124*, 024722.

(13) Han, K. N.; Bernardi, S.; Wang, L.; Searles, D. J. Water Structure and Transport in Zeolites with Pores in One or Three Dimensions from Molecular Dynamics Simulations. *J. Phys. Chem. C* **2017**, *121*, 381−391.

(14) Li, B.; Sun, X. Water Clusters with Anion Templates in Cucurbit [6] Uril Supramolecular Pseudorotaxanes. *Inorg. Chem. Commun.* **2016**, *73*, 157−160.

(15) Ghosh, S. K.; Bharadwaj, P. K. A Dodecameric Water Cluster Built Around a Cyclic Quasiplanar Hexameric Core in an Organic Supramolecular Complex of a Cryptand. *Angew. Chem., Int. Ed.* **2004**, *43*, 3577−3580.
(16) Ismail, A. E.; Grest, G. S.; Heine, D. R.; Stevens, M. J.; Tsige, M. Interfacial Structure and Dynamics of Siloxane Systems: PDMS- Vapor and PDMS- Water. *Macromolecules* **2009**, *42*, 3186−3194.
(17) Renou, R.; Ding, M.; Zhu, H.; Ghoufi, A.; Szymczyk, A. Molecular simulations of water and ion transport through nanoporous membranes. *Application of Nanotechnology in Membranes for Water Treatment (Sustainable Water Developments - Resources, Management, Treatment, Efficiency and Reuse)*; CRC Press: Boca Raton, FL, 2017; pp 213−236.
(18) Spry, D.; Goun, A.; Glusac, K.; Moilanen, D. E.; Fayer, M. Proton Transport and the Water Environment in Nafion Fuel Cell Membranes and AOT Reverse Micelles. *J. Am. Chem. Soc.* **2007**, *129*, 8122−8130.
(19) Barique, M. A.; Wu, L.; Takimoto, N.; Kidena, K.; Ohira, A. Effect of Water on the Changes in Morphology and Proton Conductivity for the Highly Crystalline Hydrocarbon Polymer Electrolyte Membrane for Fuel Cells. *J. Phys. Chem. B* **2009**, *113*, 15921−15927.
(20) Levy, Y.; Onuchic, J. N. Water Mediation in Protein Folding and Molecular Recognition. *Annu. Rev. Biophys. Biomol. Struct.* **2006**, *35*, 389−415.
(21) Yang, J.; Wang, Y.; Wang, L.; Zhong, D. Mapping Hydration Dynamics Around a β-Barrel Protein. *J. Am. Chem. Soc.* **2017**, *139*, 4399−4408.
(22) Ball, P. Water is an Active Matrix of Life for Cell and Molecular Biology. *Proc. Natl. Acad. Sci. U. S. A.* **2017**, 201703781.
(23) Tanaka, M.; Mochizuki, A.; Ishii, N.; Motomura, T.; Hatakeyama, T. Study of Blood Compatibility with Poly (2-methoxyethyl acrylate). Relationship Between Water Structure and Platelet Compatibility in Poly (2-methoxyethylacrylate-co-2-hydroxyethylmethacrylate). *Biomacromolecules* **2002**, *3*, 36−41.
(24) Heinz, H.; Jha, K. C.; Luettmer-Strathmann, J.; Farmer, B. L.; Naik, R. R. Polarization at Metal-Biomolecular Interfaces in Solution. *J. R. Soc., Interface* **2011**, *8*, 220−232.
(25) Akdogan, Y.; Wei, W.; Huang, K.-Y.; Kageyama, Y.; Danner, E. W.; Miller, D. R.; Martinez Rodriguez, N. R.; Waite, J. H.; Han, S. Intrinsic Surface-Drying Properties of Bioadhesive Proteins. *Angew. Chem., Int. Ed.* **2014**, *53*, 11253−11256.
(26) Chen, J.; Dou, R.; Cui, D.; Zhang, Q.; Zhang, Y.; Xu, F.; Zhou, X.; Wang, J.; Song, Y.; Jiang, L. Robust Prototypical Anti-Icing Coatings with a Self-Lubricating Liquid Water Layer between Ice and Substrate. *ACS Appl. Mater. Interfaces* **2013**, *5*, 4026−4030.
(27) Jha, K. C.; Anim-Danso, E.; Bekele, S.; Eason, G.; Tsige, M. On Modulating Interfacial Structure towards Improved Anti-Icing Performance. *Coatings* **2016**, *6*, 3.
(28) Dou, R.; Chen, J.; Zhang, Y.; Wang, X.; Cui, D.; Song, Y.; Jiang, L.; Wang, J. Anti-Icing Coating with an Aqueous Lubricating Layer. *ACS Appl. Mater. Interfaces* **2014**, *6*, 6998−7003.
(29) Al-Hobaib, A.; AL-Sheetan, K. M.; El Mir, L. Effect of Iron Oxide Nanoparticles on the Performance of Polyamide Membrane for Ground Water Purification. *Mater. Sci. Semicond. Process.* **2016**, *42*, 107−110.
(30) Ma, X.; Anand, D.; Zhang, X.; Tsige, M.; Talapatra, S. Carbon Nanotube-Textured Sand for Controlling Bioavailability of Contaminated Sediments. *Nano Res.* **2010**, *3*, 412−422.
(31) Jha, K. C.; Liu, Z.; Vijwani, H.; Nadagouda, M.; Mukhopadhyay, S. M.; Tsige, M. Carbon Nanotube Based Groundwater Remediation: The Case of Trichloroethylene. *Molecules* **2016**, *21*, 953.
(32) Quemener, D.; Upadhyaya, L.; Semsarilar, M.; Deratani, A. Nanocomposite Membranes with Magnesium, Titanium, Iron and Silver Nanoparticles-A Review. *J. Memb. Sci. Res.* **2017**, *3*, 187−198.
(33) Ayirala, S. C.; Saleh, S. H.; Yousef, A. A. Microscopic Scale Study of Individual Water Ion Interactions at Complex Crude Oil-Water Interface: A New SmartWater Flood Recovery Mechanism. In *SPE Improved Oil Recovery Conference*, Tulsa, OK, April 11−13, 2016; Society of Petroleum Engineers, 2016; SPE-179590-MS.
(34) Jha, K. C.; Singh, V.; Tsige, M. In *New Frontiers in Oil and Gas Exploration*; Springer: Basel, Switzerland, 2016; pp 257−283.
(35) Liu, B.; Shi, J.; Wang, M.; Zhang, J.; Sun, B.; Shen, Y.; Sun, X. Reduction in Interfacial Tension of Water-Oil Interface by Supercritical CO 2 in Enhanced Oil Recovery Processes Studied with Molecular Dynamics Simulation. *J. Supercrit. Fluids* **2016**, *111*, 171−178.
(36) Hanot, S.; Lyonnard, S.; Mossa, S. Sub-diffusion and Population Dynamics of Water Confined in Soft Environments. *Nanoscale* **2016**, *8*, 3314−3325.
(37) Bhatta, R. S.; Yimer, Y. Y.; Tsige, M.; Perry, D. S. Conformations and Torsional Potentials of Poly (3-hexylthiophene) Oligomers: Density Functional Calculations up to the Dodecamer. *Comput. Theor. Chem.* **2012**, *995*, 36−42.
(38) Yimer, Y. Y.; Dhinojwala, A.; Tsige, M. Interfacial Properties of Free-standing Poly (3-hexylthiophene) Films. *J. Chem. Phys.* **2012**, *137*, 044703.
(39) Bhatta, R. S.; Yimer, Y. Y.; Perry, D. S.; Tsige, M. Improved Force Field for Molecular Modeling of Poly (3-hexylthiophene). *J. Phys. Chem. B* **2013**, *117*, 10035−10045.
(40) Yimer, Y. Y.; Yang, B.; Bhatta, R. S.; Tsige, M. Interfacial and Wetting Properties of Poly (3-hexylthiophene)-Water Systems. *Chem. Phys. Lett.* **2015**, *635*, 139−145.
(41) Fritz, D.; Harmandaris, V. A.; Kremer, K.; van der Vegt, N. F. Coarse-grained Polymer Melts Based on Isolated Atomistic Chains: Simulation of Polystyrene of Different Tacticities. *Macromolecules* **2009**, *42*, 7579−7588.
(42) François, J.; Gan, J.; Sarazin, D.; Guenet, J.-M. Relation Between Physical Gelation and Tacticity in Polystyrene. *Polymer* **1988**, *29*, 898−903.
(43) Huang, C.-L.; Chen, Y.-C.; Hsiao, T.-J.; Tsai, J.-C.; Wang, C. Effect of Tacticity on Viscoelastic Properties of Polystyrene. *Macromolecules* **2011**, *44*, 6155−6161.
(44) Min, K.; Paul, D. Effect of Tacticity on Permeation Properties of Poly (methyl methacrylate). *J. Polym. Sci., Part B: Polym. Phys.* **1988**, *26*, 1021−1033.
(45) Zhu, H.; Jha, K. C.; Bhatta, R. S.; Tsige, M.; Dhinojwala, A. Molecular Structure of Poly (methyl methacrylate) Surface. i. Combination of Interface-Sensitive Infrared-Visible Sum Frequency Generation, Molecular Dynamics Simulations, and Ab Initio Calculations. *Langmuir* **2014**, *30*, 11609−11618.
(46) Jha, K. C.; Zhu, H.; Dhinojwala, A.; Tsige, M. Molecular structure of poly (methyl methacrylate) surface ii: Effect of stereoregularity examined through all-atom molecular dynamics. *Langmuir* **2014**, *30*, 12775−12785.
(47) Jha, K. C.; Dhinojwala, A.; Tsige, M. Local Structure Contributions to Surface Tension of a Stereoregular Polymer. *ACS Macro Lett.* **2015**, *4*, 1234−1238.
(48) Jha, K. C.; Bekele, S.; Dhinojwala, A.; Tsige, M. Hydrogen bond directed surface dynamics at tactic poly (methyl methacrylate)/water interface. *Soft Matter* **2017**, *13*, 8556−8564.
(49) Grohens, Y.; Brogly, M.; Labbe, C.; David, M.-O.; Schultz, J. Glass Transition of Stereoregular Poly (methyl methacrylate) at Interfaces. *Langmuir* **1998**, *14*, 2929−2932.
(50) Soldera, A. Comparison Between the Glass Transition Temperatures of the Two PMMA Tacticities: A Molecular Dynamics Simulation Point of View. *Macromol. Symp.* **1998**, *133*, 21−32.
(51) Lukose, B.; Bobbili, S. V.; Clancy, P. Factors Affecting Tacticity and Aggregation of P3HT Polymers in P3HT: PCBM Blends. *Mol. Simul.* **2017**, *43*, 743−755.
(52) Hillman, A. R.; Efimov, I.; Skompska, M. Time- Temperature Superposition for Viscoelastic Properties of Regioregular Poly (3-hexylthiophene) Films. *J. Am. Chem. Soc.* **2005**, *127*, 3817−3824.
(53) Zhao, K.; Xue, L.; Liu, J.; Gao, X.; Wu, S.; Han, Y.; Geng, Y. A New Method to Improve Poly (3-hexyl thiophene)(P3HT) Crystalline Behavior: Decreasing Chains Entanglement to Promote Order-Disorder Transformation in Solution. *Langmuir* **2010**, *26*, 471−477.

DOI: 10.1021/acs.jpcc.7b09191
J. Phys. Chem. C 2018, 122, 422−428

(54) Alexiadis, O.; Mavrantzas, V. G. All-Atom Molecular Dynamics Simulation of Temperature Effects on the Structural, Thermodynamic, and Packing Properties of the Pure Amorphous and Pure Crystalline Phases of Regioregular P3HT. *Macromolecules* **2013**, *46*, 2450−2467.
(55) Koppe, M.; Brabec, C. J.; Heiml, S.; Schausberger, A.; Duffy, W.; Heeney, M.; McCulloch, I. Influence of Molecular Weight Distribution on the Gelation of P3HT and its Impact on the Photovoltaic Performance. *Macromolecules* **2009**, *42*, 4661−4666.
(56) Bronstein, H. A.; Luscombe, C. K. Externally Initiated Regioregular P3HT with Controlled Molecular Weight and Narrow Polydispersity. *J. Am. Chem. Soc.* **2009**, *131*, 12894−12895.
(57) Kayunkid, N.; Uttiya, S.; Brinkmann, M. Structural Model of Regioregular Poly (3-hexylthiophene) Obtained by Electron Diffraction Analysis. *Macromolecules* **2010**, *43*, 4961−4967.
(58) Hockney, R. W.; Eastwood, J. W. *Computer Simulation Using Particles*; Taylor & Francis: New York, 1988.
(59) Plimpton, S. Fast Parallel Algorithms for Short-Range Molecular Dynamics. *J. Comput. Phys.* **1995**, *117*, 1−19.
(60) Bjorgaard, J. A.; Köse, M. E. Theoretical Study of Torsional Disorder in Poly (3-alkylthiophene) Single Chains: Intramolecular Charge-Transfer Character and Implications for Photovoltaic Properties. *J. Phys. Chem. A* **2013**, *117*, 3869−3876.
(61) Xi, L.; Shah, M.; Trout, B. L. Hopping of Water in a Glassy Polymer Studied via Transition Path Sampling and Likelihood Maximization. *J. Phys. Chem. B* **2013**, *117*, 3634−3647.
(62) Hoque, M. N.; Basu, A.; Das, G. Cyclic Pentameric Puckered Hybrid Chloride-Water Cluster [Cl3 (H2O) 4] 3-in the Hydrophobic Architecture. *Cryst. Growth Des.* **2012**, *12*, 2153−2157.
(63) Saeed, M. A.; Wong, B. M.; Fronczek, F. R.; Venkatraman, R.; Hossain, M. A. Formation of an Amine-Water Cyclic Pentamer: A New Type of Water Cluster in a Polyazacryptand. *Cryst. Growth Des.* **2010**, *10*, 1486−1488.
(64) Chaplin, M. A Proposal for the Structuring of Water. *Biophys. Chem.* **2000**, *83*, 211−221.
(65) Rodríguez-Cuamatzi, P.; Vargas-Díaz, G.; Höpfl, H. Modification of 2D water that Contains Hexameric Units in Chair and Boat Conformations-A Contribution to the Structural Elucidation of Bulk Water. *Angew. Chem., Int. Ed.* **2004**, *43*, 3041−3044.
(66) Ludwig, R.; Appelhagen, A. Calculation of Clathrate-Like Water Clusters Including H2O-Buckminsterfullerene. *Angew. Chem., Int. Ed.* **2005**, *44*, 811−815.
(67) Wilson, D. T.; Barnes, B. C.; Wu, D. T.; Sum, A. K. Molecular Dynamics Simulations of the Formation of Ethane Clathrate Hydrates. *Fluid Phase Equilib.* **2016**, *413*, 229−234.
(68) Bampoulis, P.; Teernstra, V. J.; Lohse, D.; Zandvliet, H. J.; Poelsema, B. Hydrophobic Ice Confined between Graphene and MoS2. *J. Phys. Chem. C* **2016**, *120*, 27079−27084.
(69) Nijem, N.; Canepa, P.; Kaipa, U.; Tan, K.; Roodenko, K.; Tekarli, S.; Halbert, J.; Oswald, I. W.; Arvapally, R. K.; Yang, C.; et al. Water Cluster Confinement and Methane Adsorption in the Hydrophobic Cavities of a Fluorinated Metal-Organic Framework. *J. Am. Chem. Soc.* **2013**, *135*, 12615−12626.
(70) Richardson, J. O.; Pérez, C.; Lobsiger, S.; Reid, A. A.; Temelso, B.; Shields, G. C.; Kisiel, Z.; Wales, D. J.; Pate, B. H.; Althorpe, S. C. Concerted Hydrogen-Bond Breaking by Quantum Tunneling in the Water Hexamer Prism. *Science* **2016**, *351*, 1310−1313.
(71) Yin, H.; Hummer, G.; Rasaiah, J. C. Metastable Water Clusters in the Nonpolar Cavities of the Thermostable Protein Tetrabrachion. *J. Am. Chem. Soc.* **2007**, *129*, 7369−7377.
(72) Custelcean, R.; Afloroaei, C.; Vlassa, M.; Polverejan, M. Formation of Extended Tapes of Cyclic Water Hexamers in an Organic Molecular Crystal Host. *Angew. Chem.* **2000**, *112*, 3224−3226.
(73) Moorthy, J. N.; Natarajan, R.; Venugopalan, P. Characterization of a Planar Cyclic Form of Water Hexamer in an Organic Supramolecular Complex: An Unusual Self-Assembly of Bimesityl-3, 3′-Dicarboxylic Acid. *Angew. Chem., Int. Ed.* **2002**, *41*, 3417−3420.
(74) Mei, Z.; Xu, J.; Sun, D. O/W Nano-Emulsions with Tunable PIT Induced by Inorganic Salts. *Colloids Surf., A* **2011**, *375*, 102−108.
(75) Yimer, Y. Y.; Jha, K. C.; Tsige, M. Epitaxial Transfer through End-group Coordination Modulates the Odd−Even Effect in an Alkanethiol Monolayer Assembly. *Nanoscale* **2014**, *6*, 3496−3502.

DOI: 10.1021/acs.jpcc.7b09191
J. Phys. Chem. C 2018, 122, 422−428